Lawrence Berkeley National Laboratory
Advanced Light Source

Title
New operational mode of the pencil beam interferometry based LTP

Permalink
https://escholarship.org/uc/item/35t5901n

ISBN
978-1-5106-0316-5

Authors
Centers, Gary
Smith, Brian V
Yashchuk, Valeriy V

Publication Date
2016-09-08

DOI
10.1117/12.2238298

Copyright Information
This work is made available under the terms of a Creative Commons Attribution-NonCommercial License, availalbe at https://creativecommons.org/licenses/by-nc/4.0/

Peer reviewed

eScholarship.org Powered by the California Digital Library
University of California

New operational mode of the pencil beam interferometry based LTP

Gary Centers, Brian V. Smith, and Valeriy V. Yashchuk*
Lawrence Berkeley National Laboratory, Advanced Light Source, One Cyclotron Road, Berkeley, CA 94720, USA

ABSTRACT

The advent of fully coherent free electron laser and diffraction limited synchrotron storage ring sources of x-rays is catalyzing the development of new ultra-high accuracy metrology methods. To fully exploit the potential of these sources, metrology needs to be capable of determining the figure of an optical element with sub-nanometer height accuracy. Currently, the two most prevalent slope measuring instruments used for characterization of x-ray optics are the auto-collimator based nanometer optical measuring device (NOM) and the long trace profiler (LTP) using pencil beam interferometry. These devices have been consistently improved upon by the x-ray optics metrology community, but appear to be approaching their metrological limits. Here, we consider a novel operational mode for the LTP. The fundamental measuring principle of the LTP is reviewed, and a suggested mode of operation is analytically derived. This mode of operation leads to significant suppression of the instrumental systematic errors. Via cross-comparison measurement with the LTP in old and new modes, the performance of the profiler in the new mode is investigated. We also discuss potential areas of further development, including the possibility for local curvature measurement.

Keywords: x-ray optics, optical metrology, surface slope profilometry, LTP, pencil beam interferometry, error reduction, calibration

*Corresponding author: vvyashchuk@lbl.gov

1. INTRODUCTION

Next generation light sources are putting increasingly stringent requirements on x-ray optics which are currently ≤ 30-50 nrad root-mean-square (RMS) for surface slope variation and ≤ 0.5 nm RMS for height variation. Fabrication and optimal beamline use of such optics is the motivation for improvement of ex situ metrology [1,2].

For surface slope measurements, the two most common instruments used at synchrotron facilities are the pencil beam interferometry (PBI) based long trace profiler (LTP) [3-7] and the autocollimator based profiler (such as the NOM system at HZB/BESSY-II [8,9]) and those at various other facilities [10-14]).

Both the LTP and autocollimator based profilers essentially operate as high precision deflection sensors to measure angle. The two instruments have been consistently improved over the years and are currently capable of measuring modern x-ray optics but require ideal environmental conditions [15], optimal measurement strategies to suppress random and drift errors [16], and are system limited making accurate calibration or suppression of inherent systematic error a necessity (which is on the level of 1-2 µrad over the roughly 10 mrad dynamic range of the instruments [17-20]). With the systematic error dependent on the curvatures and sizes of the optics under test, accurate calibration of the instruments is an arduous task. This challenge has been met by the x-ray optics metrology community with a variety of comprehensive and ingenious calibration methods (see, for example, Refs. [20-25] and references therein).

With calibration of systematic error being the key to achieving higher absolute accuracies, the ease in which one can characterize and suppress the systematic error becomes critical. With the autocollimator's design and internal processing algorithms mostly proprietary, the LTP becomes the natural choice for open investigation, innovation, and development. The main caveat for the historical use of the LTP to date, and a major motivation for this investigation, is that PBI for its operation has not been a requirement, clearly demonstrated with the use of a single Gaussian beam [7,25]. In this work, initial developments for the direction of fully realizing PBI in LTP operation are reported with the use of a new mode of operation.

We present this new operational mode by first starting with a brief review of the LTP's fundamental operating principle, pencil beam interferometry. We suggest a minor change of the conventional interference pattern from two peaks to four

peaks by increasing the beam separation. This new 4-peak pattern allows the standard center minimum to be tracked as well as the additional left and right minimums.

One of the main advantages apparent is the capacity to characterize the systematic error present in the measurement, and correspondingly suppress it. This potentially bypasses the need to accurately calibrate the non-linear errors of the LTP, allowing future redesigns to easily achieve required absolute accuracies. Another potential avenue of development is the possibility for local curvature measurements from the frequency of oscillation (fringe spacing).

In summary, the paper is organized as follows: Section 2 reviews pencil beam interferometry and its application in the LTP as well as introducing the new measurement mode. Section 3 presents initial results using the 4-peak mode for measurement of a 40-m concave spherical round robin reference mirror, demonstrating suppression and characterization of systematic error. Potential capability of the 4-peak mode to provide valuable information about the surface curvature distribution is considered in Sec. 4. Section 5 is the conclusion providing a discussion of our current and future directions for development.

2. BRIEF REVIEW OF LTP MEASURING PRINCIPLE

2.1. Pencil beam interferometry

Pencil beam interferometry as a technique for profiling surfaces was initially patented by K. Von Bieren in 1985 [26-28]. Although the paper itself has some arithmetic misprints, it introduces PBI and demonstrates its first application. A brief derivation of the LTP operating principle is provided here after a description of a simplified PBI optical schematic similar to the one provided in the patent [28]. The application of the PBI in long trace profilers for precision characterization of x-ray mirror surface slope topography was first suggested and analyzed by P. Takacs et. al. [29].

In the PBI schematic proposed by K. Von Bieren (see Fig. 1), two parallel pencil beams (1, 2) are formed with a beam splitter (BS1) and a mirror. The interferometer uses a profiler schematic (see, for example Refs. [25,30]) with a movable pentaprism. The two pencil beams redirected by the second beam splitter (BS2) reflect from the optical surface under test (SUT), and pass through a Fourier transform lens (FTL). The two beams generate an interference pattern in the back focal plane of the FTL where a detector is placed for measuring the light intensity distribution. In the LTP based on PBI, the detection system outlined in the patent [28] is usually replaced with the position sensitive light detector such as a linear photodiode array or a CCD camera.

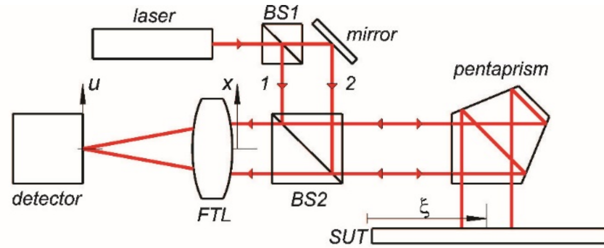

Figure 1: Simplified optical schematic of a pencil beam interferometer patented by K. Von Bieren [28]. BS1 is a beam splitter used to split the laser beam to two interfering beams 1 and 2; the beam splitter BS2 sends the beams to the surface under test, SUT, through the moving pentaprism. The reflected beams are focused with the Fourier transform lens, FTL, to the focal plane where a position sensitive detector records the intensity distribution resulting from the interference of the reflected light beams.

A brief derivation of the LTP operating principle, provided here, assumes the ideal situation free of any experimental imperfections. The two beams of light with wavelength λ (in air) have Gaussian amplitude distribution of width σ. We also assume the surface introduces a constant phase difference between the two beams described by the height of the surface.

The input amplitude distribution after reflection from the SUT can then be expressed as

$$u(x,y) = A\exp\left[-\frac{\left(x-M/2\right)^2+y^2}{2\sigma^2}\right]\exp\left[\frac{4\pi j}{\lambda}\phi(\xi-M/2)\right]+A\exp\left[-\frac{\left(x+M/2\right)^2+y^2}{2\sigma^2}\right]\exp\left[\frac{4\pi j}{\lambda}\phi(\xi+M/2)+j\pi\right], \tag{1}$$

where x, y describes the input plane directly in front of the Fourier transform lens (FTL), ξ is the position of the principal ray on the optical surface, M is the separation between the beams, $\phi(\xi \pm M/2)$ is the path length introduced by an arbitrarily shaped SUT, σ is the Gaussian width of each beam defined by $\mathrm{FWHM}/2\sqrt{2\ln 2}$, and A is the complex amplitude of the beams. The π phase shift between the beams is typical in LTP measurements to ensure a central minimum of the final interference pattern recorded by the detector. Note that the 4π in the phase exponential in Eq. (1), appearing different from the usual $k = 2\pi/\lambda$, originates from the effective doubling of the introduced path length difference after reflection (more detailed derivations can be found in Ref. [31,32]). Additionally, the convention is chosen such that $\phi(\xi \pm M/2)$ is positively (negatively) defined for convex (concave) surfaces with zero at the surface extremum.

For an input amplitude distribution $u(x, y)$ placed directly in front of a FTL, the intensity distribution in the u, v focal plane is [33]:

$$I(u,v) = \frac{A^2}{\lambda^2 f^2} \left| \int_{-\infty}^{\infty}\int u(x,y) \exp\left[-j\frac{2\pi}{\lambda f}(xu + yv) \right] dxdy \right|^2, \tag{2}$$

where f is the focal length of the FTL. (For the reader's curiosity, the origin of the name for the Fourier transform lens is apparent in the above formula, but it's only true given the quadratic phase factors of the lens transformation and Fresnel diffraction equation multiply to unity [33].)

Plugging in Eq. (1) into (2) yields the following expression for the intensity distribution in the focal plane:

$$I(u) = \frac{4\pi A^2\sigma^2}{\lambda f} \exp\left[-\frac{4\pi^2\sigma^2}{\lambda^2 f^2} u^2 \right] \left(1 - \cos\frac{4\pi}{\lambda}\left[\frac{Mu}{2f} + \phi(\xi + M/2) - \phi(\xi - M/2) \right] \right). \tag{3}$$

This can be described as an enveloping (modulation) function of a sinusoidal oscillation, similar to the classic Young's double slit interference.

This formula and approach is similarly outlined in [29]. They show that a Taylor expansion of the phase difference (where the $4\pi/\lambda$ is included in the definition of ϕ, making it a phase), $\phi(\xi + M/2) - \phi(\xi - M/2) \approx M\phi'(\xi)$, proves that the dependence is on the derivative of the phase and thus the surface slope since $\phi(\xi) = Z(\xi)$ and $Z'(\xi) \approx \alpha(\xi)$, where $Z(\xi)$ is the surface height distribution that introduces the phase difference and $\alpha(\xi)$ the slope.

For the intensity distribution given by Eq. (3), the enveloping function does not affect the minimum positions and we derive from (3) the basic expression for surface slope profiling with a PBI based sensor:

$$u_{\min,n}(\xi) = 2f\frac{\phi(\xi - M/2) - \phi(\xi + M/2)}{M} + \frac{n\lambda f}{M},\ n \in \mathbb{Z}. \tag{4}$$

Approximating the phase difference with the derivative and looking at the central minimum, $n = 0$, we arrive at:

$$u_{\min,n=0}(\xi) \approx 2f\phi'(\xi) = 2fZ'(\xi). \tag{5}$$

The relation (5) between the position of the interference pattern's central minimum, measured in the focal plane of the FTL, and the surface height derivative is usually used for explanation of the LTP measuring principle [25,34]. This relation effectively embodies both explanations of the classical deflectometric application of PBI in surface slope profilometers; being that of the changing phase of the interference pattern (4) or simply the equation above for an f-theta lens (5). Below, we show the potential advantages of modifying the classic interference pattern to utilize the previously neglected side minimums given by $n \neq 0$.

2.2. The idea of the new measuring mode

In the simplest realization, the proposed measurement mode consists in tracking (recording) the positions of the two extra side minimums of Eq. (4) given by $n = \pm 1$ (in addition to the central one) as a function of the position along the SUT ξ:

$$u_n(\xi) = 2f\,\frac{\phi(\xi - M/2) - \phi(\xi + M/2)}{M} + \frac{n\lambda f}{M},\ n = \{-1, 0, 1\}\ .$$

Figure 2 illustrates the 'classic' and 'new' interference patterns.

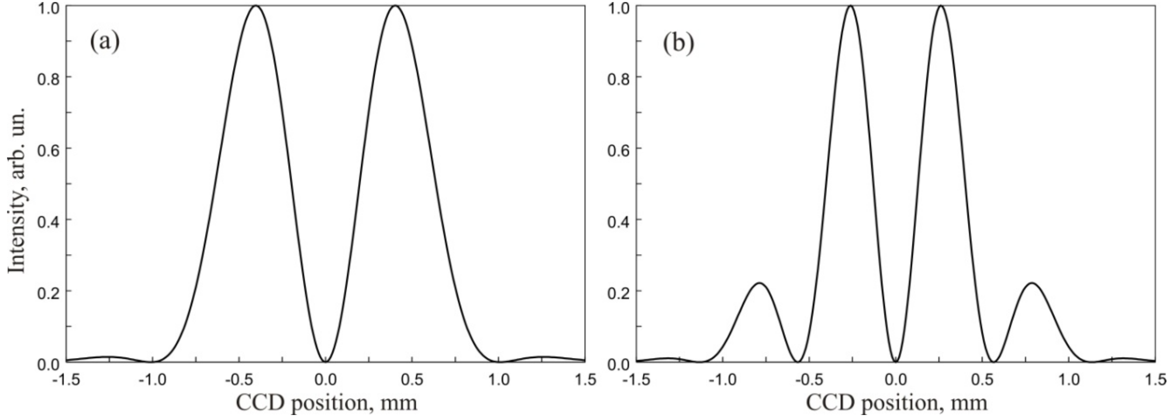

Figure 2: The two interference patterns where the conventional (a) consists of two peaks within the envelope while the newly proposed pattern (b) contains 4 peaks defining two additional minimums.

Since the separation of the $n = \pm 1$ minimum positions from the center is inversely proportional to the initial beam separation M, simply increasing M allows one to fit the side minimums within the enveloping function. For the particular LTP [5,6,35-37] at the Advanced Light Source (ALS) X-Ray Optics Laboratory (XROL) [15], the increase required was anywhere between 50-90% of its original ~0.9 mm separation (as measured at the position of the SUT).

Let us consider typical errors for measured values of the minimum positions, $u_n^M(\xi_i)$, sampled at discrete points of the SUT, $\xi_i,\ i = 1, ..., N$:

$$u_n^M(\xi_i) = u_n(\xi_i) + S(u_n(\xi_i)) + R(\xi_i) + D(\xi_i(t)),\ n = 0, \pm 1, \tag{6}$$

where the random, drift, and systematic errors are represented by $R(\xi_i)$, $D(\xi_i(t))$, and $S(u_n(\xi_i))$, respectively (see, for example, Refs. [16, 37]). With the XROL's advanced environmental conditions [15] and using optimal measurement strategies [16], both drift and random errors, $D(\xi_i(t))$ and $R(\xi_i)$, can be suppressed to negligible levels and ignored. We also define the three positions as the left, center, and right minimums, $u_{-1}, u_0, u_1 \equiv u_L, u_C, u_R$, making the measurements described by:

$$\begin{aligned} u_L^M(\xi_i) &= u_L(\xi_i) + S(u_L(\xi_i)) \\ u_C^M(\xi_i) &= u_C(\xi_i) + S(u_C(\xi_i)) \\ u_R^M(\xi_i) &= u_R(\xi_i) + S(u_R(\xi_i)), \end{aligned} \tag{7}$$

or equivalently:

$$\begin{aligned} u_L^M(\xi_i) &= \frac{2f}{M}\left[\phi(\xi_i - M/2) - \phi(\xi_i + M/2)\right] - \frac{\lambda f}{M} + S_L(\xi_i) \\ u_C^M(\xi_i) &= \frac{2f}{M}\left[\phi(\xi_i - M/2) - \phi(\xi_i + M/2)\right] + S_C(\xi_i) \\ u_R^M(\xi_i) &= \frac{2f}{M}\left[\phi(\xi_i - M/2) - \phi(\xi_i + M/2)\right] + \frac{\lambda f}{M} + S_R(\xi_i). \end{aligned} \tag{8}$$

The exact relationship between the three minimum's systematic errors is currently unknown and they are likely not related by a translation of the central systematic error as Eq. (7) indirectly implies. The interpretation of systematic error as being mapped to specific points on the detector plane (u, v) (i.e. for different alignments and paths through the optics) is only true for each point of the pattern individually; the focal plane distribution of the error point by point can, in practice, be quite complicated.

For the LTP in particular, systematic error is mainly introduced by inhomogeneities in material of the bulk optics (beam splitters, FTL), their fabrication imperfections, and the surface imperfections of the folding mirrors after the lens. The systematic errors that originate before the lens are introduced to each beam individually, sampled from the optics at the beam separation and linearly contribute to the recorded slope distribution; however, the character of the contribution for the errors that accumulate during focusing is more complicated. It is important to note that phase errors introduced to each beam (which would be introduced inside the brackets of Eq. (8), but are currently absorbed in $S_{L,C,R}(\xi_i)$) appear as a difference in the final measurement of minimum position. Thus, any phase perturbations comparable in spatial frequency to the beam separation are naturally removed, and correlated errors between the beams suppressed. This would not be true when using a single beam, where no such systematic error suppression would naturally occur. This is likely the explanation for observed increased noise seen when using a single Gaussian beam (i.e. no suppression of convection noise between the beams) [25].

Given that the errors are different and weakly correlated between the three minimums (these assumptions have to be verified experimentally; see Sec. 3), an average of the left and right slope measurements should reproduce the central measurement with suppressed systematic error, where the magnitude of suppression depends on the cross-correlation properties of the errors. The equation for the left/right (LR) average for a spherical optic can then be described by

$$u_{LRavg}^{M}(\xi_i) = \frac{u_L^M(\xi_i) + u_R^M(\xi_i)}{2} = -\frac{2f\xi_i}{R_{fit}} + \frac{1}{k}\delta\alpha(\xi_i) + \frac{S_L(\xi_i) + S_R(\xi_i)}{2}, \tag{9}$$

where R_{fit} is the best fit spherical radius of curvature, k is the distance to slope conversion factor determined through linear calibration which is approximately $(\text{pixel size})/2f$, and $\delta\alpha(\xi_i)$ is the residual slope deviation from the best fit curvature.

This article is a first investigation into the relationship between the systematic errors of the three minimums and the benefits of this new mode, in general. If indeed this provides a method for systematic error suppression, further development could potentially weaken the requirements to non-linear calibration at the measurement accuracies needed for next generation x-ray mirrors. In Sec. 3 below, the 4-peak mode is demonstrated through measurements of the 40-m concave spherical reference mirror.

3. MEASUREMENTS WITH A 40-M SPHERICAL MIRROR

3.1. Setup and measurement description

Here we describe three different measurements performed over a clear aperture of ~300 mm about the center of the 40-m concave spherical uncoated mirror using 1 mm increments. (Note that the same mirror was used for the round robin test of surface slope profiles around the world [38].) The second measurement was performed to confirm repeatability while the third was performed after tilting the substrate ~930 µrad with respect to the detector and tangential (lengthwise) direction of the SUT. Each measurement was an average of 8 scans performed using the optimal scanning strategy to remove drift and random error [16]. The experimental arrangement is depicted in Fig. 3.

The measurements were all set at the previously calibrated height of 252 mm from the LTP granite table (see Ref. [24]). Additionally, a DALSA CCD and flat reference mirror were set up at the same height to image the initial separation M and corresponding interference pattern from flat surface respectively. These measurements were only performed before the 1st measurement since the separation, and corresponding interference pattern, should remain approximately constant as long as the mechanical/thermal drift between measurements is adjusted appropriately.

Due to the changing distance of the LTP reference channel, any off-parallelism between the LTP light beams will introduce spurious curvature to the measurement. A diverging pair of beams will pinch the reference channel interference minimums as distance is increased, shown diagrammatically in Fig. 4.

Since the carriage wobble and pointing instability are still reproduced by the three reference minimums individually despite introduced divergence, we can use the central minimum as a reference for the three sample channel minimums to avoid the addition of spurious radius of curvature in the measurement. It should be noted that measurements with a 300 mm long flat mirror revealed a divergence of ~40 µrad of the reference channel beams for the XROL's LTP.

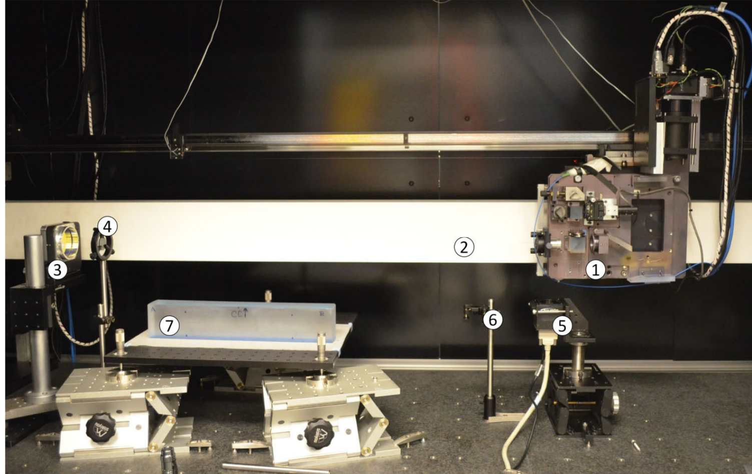

Figure 3: Experimental arrangement for 4-peak mode investigation with 40-m concave spherical mirror. (1) is the LTP optical head, (2) is the ceramic gantry, (3) is the LTP reference channel mirror, (4) is a neutral density filter, (5) is a DALSA CCD, (6) is a reference flat, (7) is the 40-m spherical mirror.

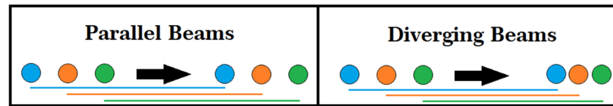

Figure 4: The effective changes to the 3 minimum positions on the CCD at the beginning (left) and end (right) of the measurements with the parallel (top) and diverging (bottom) mutual alignment of the LTP beams. The blue (left), orange (central), and green (right) circles correspond to the left, center, and right minimums, respectively. Color available online.

3.2. Measurement Results

A summary of the results presented in this section are the residual slope distributions (after subtraction of the best fit spherical surface) for the un-tilted and tilted measurements (Sec. 3.2.1), repeatability between the first and second measurement (Sec. 3.2.2), and a comparison of the LR average to center slope (Sec. 3.2.3).

3.2.1. Slope distributions of the three minimums

The left, center, and right measured slopes, determined by a subtraction of the center reference channel trace from that of the three sample traces as discussed in the previous section, are shown in Fig. 5 and 6 for the first un-tilted and the third tilted measurements, respectively.

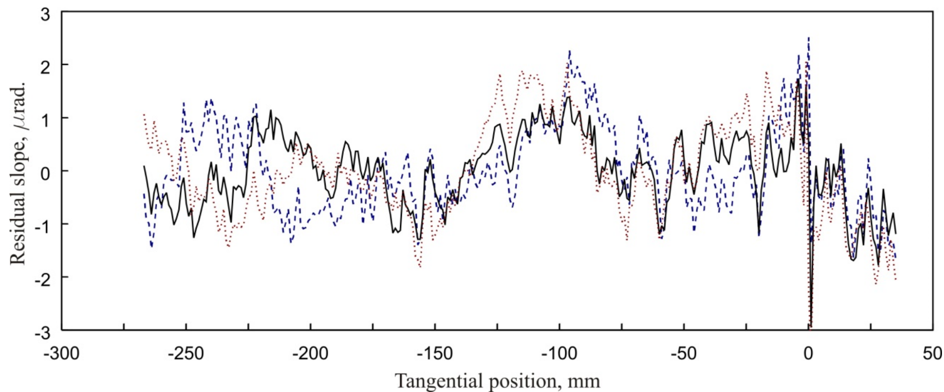

Figure 5: The residual, after subtraction of best fit line, slope variations as determined from the positions of the left (blue, dashed), center (black, solid) and right (red, dotted) minimums in the first measurement. The corresponding values of the best fit curvatures and residual RMS variations are 820 nrad, 700 nrad, 920 nrad and 40.11 m, 40.11 m, and 40.12 m respectively. The apparently different low frequency perturbations strongly affect the resulting residual RMS, which the left and right slopes appear to have increased magnitude than that of the center.

Figure 6 depicts the results of the third measurement, which was performed after tilting by 930 μrad to shift systematic error [18-20,24].

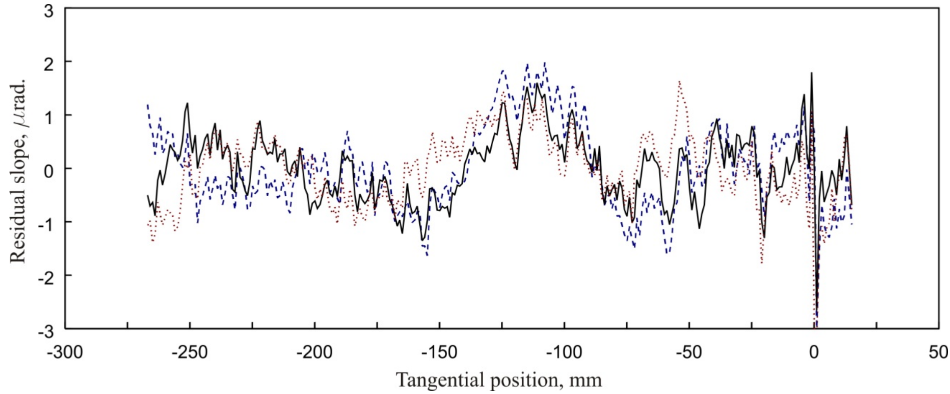

Figure 6: Plot of the residual, after subtraction of best fit line, slope variation for the measurement tilted by 930 μrad with respect to the first two. The corresponding values of the best fit curvatures and residual RMS variations for the left (blue, dashed), center (black, solid), and right (red, dotted) slopes are 810 nrad, 630 nrad, 690 nrad and 40.12 m, 40.12 m, and 40.12 m, respectively..

The measurements show that the three minimums all record slightly different residual slopes and that a tilt of the surface with respect to the detector noticeably perturbs all three recorded traces. In Sec. 3.3 we empirically show that these differences strongly correlate with the systematic error of the LTP measured in a particular calibration experiment [24].

3.2.2. 4-Peak mode repeatability

Repeatability of the measurements with the LTP in the 4-peak mode is illustrated in Fig. 7, where a difference between the first measurement and the second one, performed at the same experimental arrangement two days later, is shown.

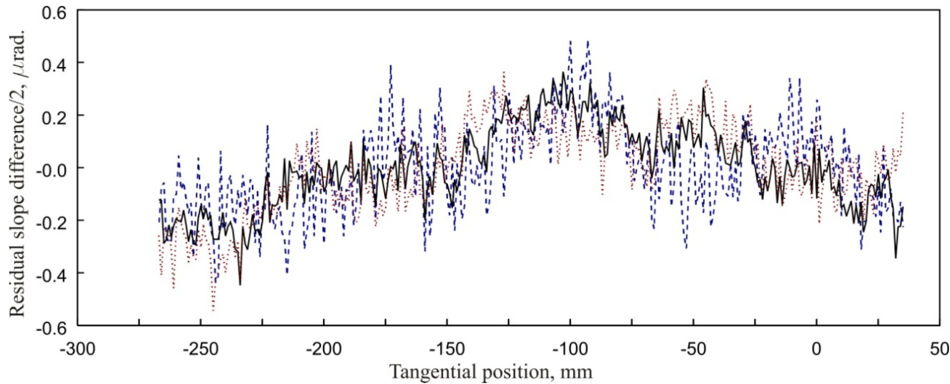

Figure 7: Repeatability of the first two measurements with the LTP in the 4-peak mode, illustrated with the difference of the three slope traces obtained using the dependence of the corresponding fringe pattern minimums on the tangential position along the 40-m spherical mirror. The left (blue, dashed), center (black, solid), and right (red, dotted) results all show expected levels of LTP RMS repeatability at 170 nrad, 160 nrad, and 170 nrad, respectively.

The repeatability for all three minimums is typical for a single run of the XROL's LTP consisting of 8 scans in the forward and reverse direction. The left minimum slope seems to have slightly increased high frequency variation; this could either be due to the direction of phase drift during measurement or a slightly different beam distribution after two days.

3.2.3. Center slope trace compared to the LR average

In Figs. 8 and 9, a comparison between the LR average and the center slope traces are shown where better coincidence than the left and right slope traces individually is apparent (compare to Figs. 5, 6). For the tilted measurement (Fig 9), the LR average and the center slopes differ by ~250 nrad RMS (taking the difference of their respective RMS quadratically). The difference can be due to the nature of the systematic error present in the measurements, which is discussed in the next section.

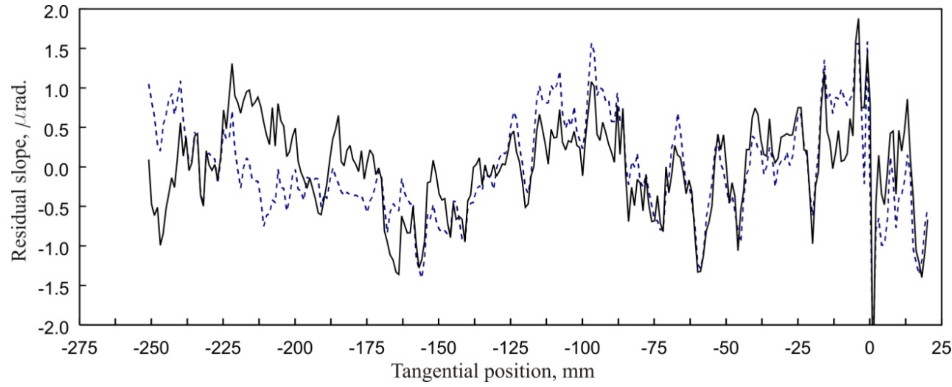

Figure 8: The residual slope variations for the center (black, solid) and LR average (blue, dashed) for the second measurement. The center, LR average trace's residual RMS and best fit curvatures are 600 nrad, 630 nrad and 40.11 m, 40.11 m, respectively.

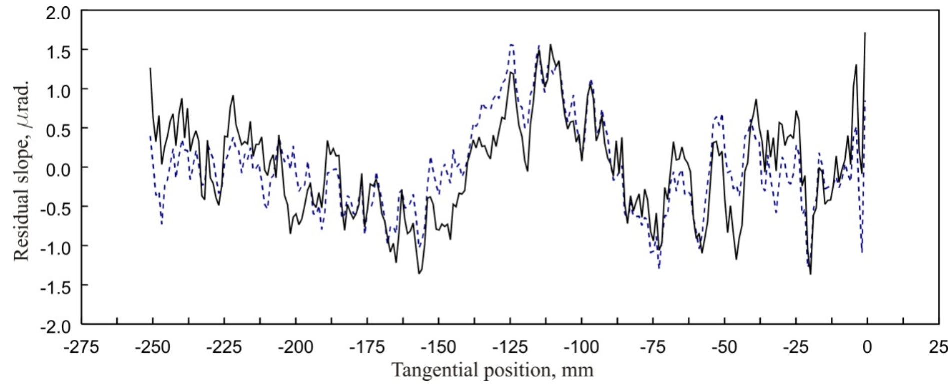

Figure 9: The residual slope variations for the center (black, solid) and LR average (blue, dashed) for the tilted measurement. The center, LR average trace's residual RMS and best fit curvatures are 630 nrad, 580 nrad and 40.12 m, 40.12 m, respectively.

3.3. Measurements in the 'traditional' and 'new' modes and the LTP systematic error

A previous calibration of the LTP, discussed in detail in [24], is used as a representation of the expected systematic error in these measurements (Sec. 3.3.1). The corresponding regions of the LTP dynamic range, used for the un-tilted and tilted measurements, illustrate the expected translation of the systematic error across the tangential position of the measurement. However, we should note significant differences between the experimental arrangements for the calibration made via tilting a flat gold-coated reference mirror and the measurements here with a 40-m spherical uncoated mirror. Besides the difference in shape of the mirrors, the initial separation of the LTP pencil beams is different (as discussed above), as well as a slight change of ~140 μrad in the roll angular alignment (sagittal position of the interference pattern on the CCD).

In Sec. 3.3.2, the main result, showing a difference between the LR average and center slope, proves that the systematic error has been suppressed in the average. It appears that the error removed is strongly correlated with the representative error from the previous calibration with slightly different alignment and beam separation.

3.3.1. The LTP systematic error

Figure 10 reproduces the LTP calibration [24] performed near the same experimental arrangement. The calibrations corresponding to the angular ranges used in the three measurements with the 40-m spherical mirror, discussed in Sec. 3.2, are shown. Note, the angular range is determined by the pixel position on the detector multiplied by the linear pixel-to-slope conversion factor. The non-linear corrections for the central slope across the CCD at 3100 pixel value (alignment of the sample channel during calibration) are shown.

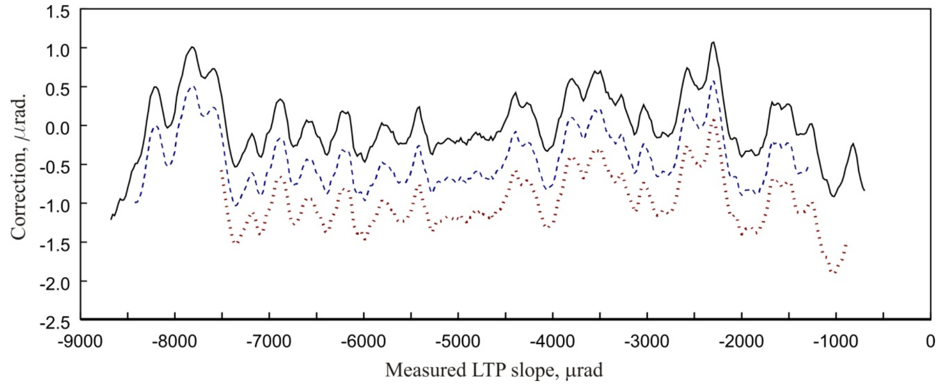

Figure 10: The previously determined LTP calibration (black, solid) and the corresponding range of the LTP detector used for the first two measurements (blue, dashed) and tilted measurement (red, dotted).

Note that the calibration in Fig. 10 cannot be directly applied to correct the measurements since they were performed not only at a different pixel position, but with a flat reference mirror and different beam separation, M . However, because the low spatial frequency LTP non-linearity tends to change slowly over the vertical position of the CCD detector, the previously measured calibration can still be used as a decent representation of the expected errors in the present measurements.

3.3.2. 4-Peak systematic error recovery

In Figs. 11 and 12, the difference between the center and LR average slope traces from the tilted and un-tilted measurements are compared to the corresponding LTP calibration corrections in Fig. 10.

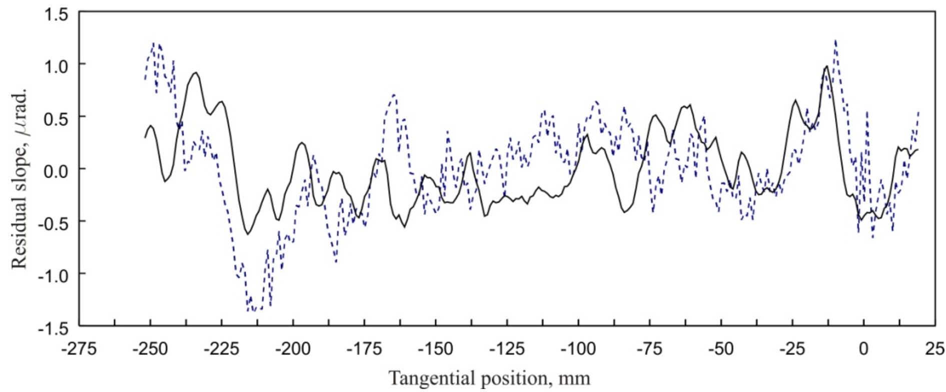

Figure 11: The difference between the center and LR average slope traces for the first un-tilted measurement (blue, dashed). For comparison, the corrections to the center measurement if they were applied (black, solid) show similar properties to the difference. The RMS variation of the recovered error is 490 nrad compared to that of the expected corrections with 360 nrad.

The difference of the center and LR average slope traces in Fig. 11 has reproduced some characteristic features of the expected LTP systematic error in the first two measurements.

Tilt of the mirror leads to a significant change of the systematic error, as seen in Fig. 10. As seen in Fig 12, this change has been captured by the difference of the center and LR average slope traces. This suggests that this LR average slope trace is significantly free of the systematic error characteristic of the central trace.

The empirically observed correlation between the LTP systematic error, measured in a dedicated experiment [14], and the difference between the traces measured in the 4-peak mode can be quantified with cross-correlation analysis. The resulting cross-correlation coefficient for the un-tilted measurements is 0.40 with a -3.7 mm lag. For the tilted measurement, a coefficient of 0.46 is determined with a 4.5 mm lag. The nonzero lag is probably due to the slightly different arrangements of the measurement set-ups, specifically the different beam separation used (where only one beam is shifted to adjust the spacing using one of the two roof prisms [6]) and the sagittal alignment discussed above.

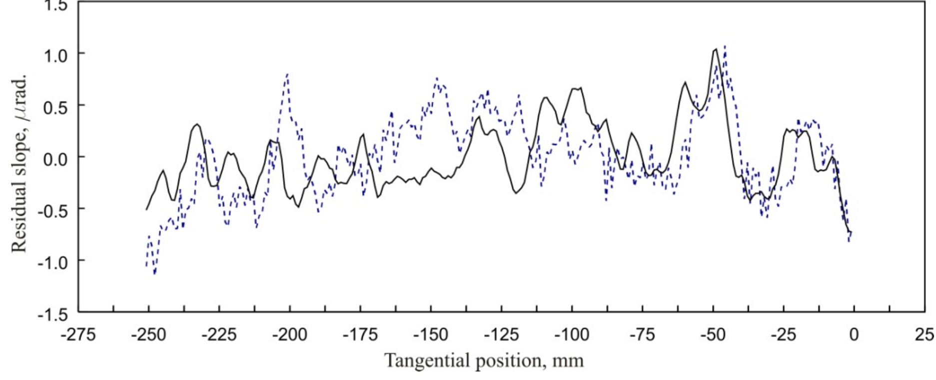

Figure 12: The difference between the center and LR average slope traces for the first tilted measurement (blue, dashed). The coincidence to the corrections to the center measurement if they were applied (black, solid) remains even after translation via tilting. The RMS variation of the recovered error is 400 nrad compared to that of the expected corrections with 330 nrad.

4. CURVATURE DEPENDENCE OF FRINGE SEPARATION

Here, we discuss a fringe separation dependence on local SUT curvature appearing due to the focusing (defocusing) nature of a concave (convex) reflective surface added to the optical system. We point out that with an appropriate calibration, a direct measurement of the difference between the left and right slope traces can provide valuable information about SUT curvature distribution.

4.1. Theory

When measuring a curved SUT using a PBI based set-up, the focusing property of the SUT has to be accounted for in the optical schematic. This focusing effect can be described with an effective separation at the input of the FTL, M_{eff}, that depends on the SUT curvature, initial separation between the beams, and distance between SUT and lens which for now we consider constant.

The effective fringe separation can be obtained from the equations (8) by taking the difference between the right and left slopes. Considering the ideal situation free of systematic errors the difference yields:

$$u_R(\xi) - u_L(\xi) = \frac{2\lambda f}{M} = \frac{2\lambda f}{M_{eff}(M_0, R(\xi))}. \tag{10}$$

The local curvature, $R(\xi)$, defined over the initial beam separation M_0 on the surface, can potentially be extracted.

One can also treat the SUT as an additional focusing element and use the simple equation:

$$f_{eff}(\xi) = \left(\frac{1}{f} + \frac{2}{R(\xi)}\right)^{-1} = \frac{fR(\xi)}{R(\xi)+2f} \approx f\left(1 - \frac{2f}{R(\xi)}\right), \tag{11}$$

where the approximation is only true for $f \ll R(\xi)$. Thus, we can write the equivalent expression:

$$R(\xi) \approx \frac{4\lambda f^2}{2\lambda f - M_0\left[u_R(\xi) - u_L(\xi)\right]}. \tag{12}$$

that connect the local radius of curvature and the separation between the left and right minimums.

4.2. Measurement of the side minimum separation on mirror curvature

The intensity distribution of the LTP sample beams was measured using a DALSA CCD placed at the same height as that of the 40-m spherical mirror (see Fig. 3). After sagittal averaging of the beam distributions to reduce to 1-D, a Gaussian fit was performed to determine the initial separation M =1.5332 mm. The beams also differed in amplitude by ~30% which partially explains the background [32] raising the minimums in Fig. 13.

The interference patterns on the LTP CCD from both the reference flat and 40-m spherical mirror were also recorded. Their distributions after vertical averaging are shown in Fig. 13. The observed difference between the separations of the side minimums for the flat and 40-m spherical mirrors was 57 µm.

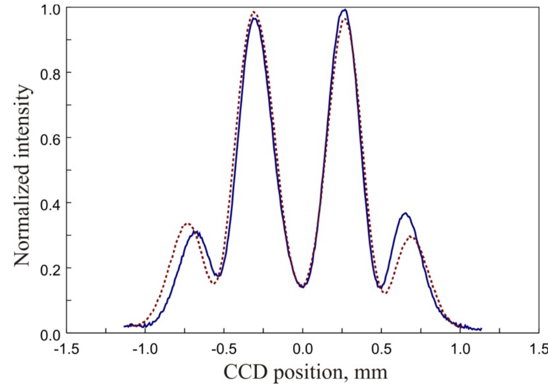

Figure 13: Plot of the interference patterns form the reference flat and 40-m mirrors after sagittal averaging. The fringe separation for the flat substrate was determined to be 1.101 mm while the 40 m separation was 1.044 mm.

The curvature effects are seen as a decrease in the fringe separation as well as changes to the shape and height of the side peaks. The observation requires further investigation to determine if the relationship between curvature and the fringes agree with the discussion in Sec. 4.1.

5. CONCLUSION

In this article, we have reviewed pencil beam interferometry and suggested a new 4-peak mode of operation for the pencil-beam-interferometry based long trace profiler. In the course of LTP measurements in the 4-peak mode, the positions of three minimums (with two side minimums additional to the conventional central minimum) of the interference pattern are determined and recorded to simultaneously provide three surface slope traces.

We have presented initial investigation of the new mode through measurements of the 40-m spherical concave mirror and experimentally demonstrated a significant suppression of the LTP systematic error when the surface slope trace is measured from an average of the two slope traces determined by the left and right side minimums.

We have provided an analytic expression showing natural suppression of systematic and random variation from the difference of phase between two beams, in contrast to the use of a single beam. Additionally, the suppression of uncorrelated errors through averaging fringe pattern minimums has been confirmed, but an analytic description of this effect is desired given the observed efficacy.

A better understanding of the different relationship of surface slope and systematic contributions between both the phase and angular distributions should provide direction to a next generation slope sensor.

6. ACKNOWLEDGEMENT

The Advanced Light Source is supported by the Director, Office of Science, Office of Basic Energy Sciences, Material Science Division, of the U.S. Department of Energy under Contract No. DE-AC02-05CH11231 at Lawrence Berkeley National Laboratory.

This document was prepared as an account of work sponsored by the United States Government. While this document is believed to contain correct information, neither the United States Government nor any agency thereof, nor The Regents of the University of California, nor any of their employees, makes any warranty, express or implied, or assumes any legal responsibility for the accuracy, completeness, or usefulness of any information, apparatus, product, or process disclosed, or represents that its use would not infringe privately owned rights. Reference herein to any specific commercial product, process, or service by its trade name, trademark, manufacturer, or otherwise, does not necessarily constitute or imply its endorsement, recommendation, or favoring by the United States Government or any agency thereof, or The Regents of the University of California. The views and opinions of authors expressed herein

do not necessarily state or reflect those of the United States Government or any agency thereof or The Regents of the University of California.

REFERENCES

[1] M. Idir and V. V. Yashchuk, Co-Chairs, “Optical and X-ray metrology,” in: X-ray Optics for BES Light Source Facilities, Report of the Basic Energy Sciences Workshop on X-ray Optics for BES Light Source Facilities, D. Mills and H. Padmore, Co-Chairs, pp. 44-55, U.S. Department of Energy, Office of Science, Potomac, MD (March 27-29, 2013); <http://science.energy.gov/~/media/bes/pdf/reports/files/BES_XRay_Optics_rpt.pdf>.

[2] P. Z. Takacs, “X-ray optics metrology,” in: Handbook of Optics, 3rd ed., Vol. V, M. Bass, Ed., Chapter 46, McGraw-Hill, New York (2009)

[3] E. L. Church, P. Z. Takacs, “Use of an optical profiling instrument for the measurement of the figure and finish of optical quality surfaces,” Wear 109, 241-57 (1986).

[4] P. Z. Takacs, S. Qian, J. Colbert, “Design of a long trace surface profiler,” SPIE Proc. 749 (1987), 59-64.

[5] S. C. Irick, W. R. McKinney, D. L. J. Lunt, and P. Z. Takacs, “Using a straightness reference in obtaining more accurate surface profiles from a long trace profiler,” Rev. Sci. Instrum. 63, 1436 (1992); http://dx.doi.org/10.1063/1.1143036.

[6] J. L. Kirschman, E. E. Domning, W. R. McKinney, G. Y. Morrison, B. V. Smith, and V. V. Yashchuk, Performance of the upgraded LTP-II at the ALS Optical Metrology Laboratory, Proc. SPIE 7077, 70770A/1-12 (2008).

[7] Y. Senba, H. Kishimoto, H. Ohashi, H. Yumoto, T. Zeschke, F. Siewert, S. Goto, and T. Ishikawa, “Upgrade of long trace profiler for characterization of high-precision X-ray mirrors at SPring-8,” Nucl. Instr. and Meth. **A 616**(2-3), 237-240 (2010).

[8] F. Siewert, T. Noll, T. Schlegel, T. Zeschke, and H. Lammert, “The Nanometre Optical Component Measuring Machine: a new Sub-nm Topography Measuring Device for X-ray Optics at BESSY,” AIP Conference Proceedings 705, 847-850 (2004).

[9] F. Siewert, J. Buchheim, T. Zeschke, M. Störmer, G. Falkenberg and R. Sankari, On the characterization of ultra-precise X-ray optical components: advances and challenges in ex situ metrology, J. Synchrotron Rad. 21, 968–975 (2014); doi:10.1107/S1600577514016221

[10] V. V. Yashchuk, S. Barber, E. E. Domning, J. L. Kirschman, G. Y. Morrison, B. V. Smith, F. Siewert, T. Zeschke, R. Geckeler, and A. Just, “Sub-microradian surface slope metrology with the ALS Developmental Long Trace Profiler,” Nucl. Instr. and Meth. A 616(2-3), 212-223 (2010).

[11] S.G. Alcock, K.J.S. Sawhney, S. Scott, U. Pedersen, R. Walton, F. Siewert, T. Zeschke, F. Senf, T. Noll and H. Lammert, “The Diamond-NOM: A non-contact profiler capable of characterizing optical figure error with sub-nanometre repeatability,” Nucl. Instr. Meth. A 616(2-3), 224-228 (2010).

[12] J. Nicolas and J. C. Martınez, “Characterization of the error budget of Alba-NOM,” Nucl. Instr. and Meth. A 710, 24-30 (2013).

[13] I. Lacey, N. A. Artemiev, E. E. Domning, W. R. McKinney, G. Y. Morrison, S. A. Morton, B. V. Smith, and V. V. Yashchuk, “The developmental long trace profiler (DLTP) optimized for metrology of side-facing optics at the ALS,” Proc. SPIE 9206, 920603/1-11 (2014); doi:10.1117/12.2061969.

[14] S. Qian, R. D. Geckeler, A. Just, M. Idir, and X. Wu, “Approaching sub-50 nanoradian measurements by reducing the saw-tooth deviation of the autocollimator in the Nano-Optic-Measuring Machine,” Nucl. Instr. and Meth. A 785, 206-212 (2015).

[15] V. Yashchuk, N. A. Artemiev, I. Lacey, W. R. McKinney, and H. A. Padmore, “Advanced environmental control as a key component in the development of ultra-high accuracy ex situ metrology for x-ray optics,” Opt. Eng. 54(10), 104104/1-14 (2015); doi: 10.1117/1.OE.54.10.104104.

[16] V. V. Yashchuk, “Optimal Measurement Strategies for Effective Suppression of Drift Errors,” Rev. Sci. Instrum. 80, 115101-1-10 (2009); http://dx.doi.org/10.1063/1.3249559.

[17] R. D. Geckeler and A. Just, “Optimized use and calibration of autocollimators in deflectometry,” Proc. SPIE 6704, 670407/1-12 (2007).

[18] F. Polack, M. Thomasset, S. Brochet, and A. Rommeveaux, “An LTP stitching procedure with compensation of instrument errors: Comparison of SOLEIL and ESRF results on strongly curved mirrors,” Nucl. Instr. and Met. A 616(2-3), 207-211 (2010).

[19] V. V. Yashchuk, N. A. Artemiev, I. Lacey, and D. J. Merthe, "Correlation analysis of surface slope metrology measurements of high quality x-ray optics," Proc. SPIE 8848, 88480I-1-15 (2013); doi: 10.1117/12.2024694.
[20] R. D. Geckeler, A. Just, "A shearing-based method for the simultaneous calibration of angle measuring devices," Meas. Sci. and Tech. **25**, 105009 (2014); DOI: 10.1088/0957-0233/25/10/105009.
[21] F. Siewert, J. Buchheim, and T. Zeschke, "Characterization and calibration of 2nd generation slope measuring profiler," Nucl. Instrum. Meth. **A616**, 119–27 (2010); doi:10.1016/j.nima.2009.12.033
[22] S. G. Alcock, A. Bugnar, I. Nistea, K. Sawhney, S. Scott, M. Hillman, J. Grindrod, and I. Johnson, "A novel instrument for generating angular increments of 1 nanoradian," Rev. Sci. Instrum. 86, 125108 (2015); http://dx.doi.org/10.1063/1.4937352.
[23] O. Kranz, R. D. Geckeler, A. Just, M. Krause, and W. Osten, "From plane to spatial angles: PTB's spatial angle autocollimator calibrator," Adv. Opt. Tech. **4**(5-6), 397–411 (2015); DOI: 10.1515/aot-2015-0017.
[24] V. V. Yashchuk, N. A. Artemiev, G. Centers, A. Chaubard, R. D. Geckeler, I. Lacey, H. Marth, W. R. McKinney, T. Noll, F. Siewert, M. Winter, and T. Zeschke, "High precision tilt stage as a key element to universal test mirror for characterization and calibration of slope measuring instruments," Rev. Sci. Instrum. 87(5), 051904 (2016); doi: 10.1063/1.4950729.
[25] S. Qian, G. Sostero, and P. Z. Takacs, "Precision calibration and systematic error reduction in the long trace profiler," Opt. Eng. **39**(1), 304-310 (2000); doi: 10.1117/1.602364.
[26] K. von Bieren, "Pencil Beam Interferometer For Aspherical Optical Surfaces," Proc. SPIE 343, 101 (1982); doi:10.1117/12.933743.
[27] K. von Bieren, "Interferometry of wave fronts reflected off conical surfaces," Appl. Opt. 22, 2109-2114 (1983); doi: 10.1364/AO.22.002109.
[28] K. Von Bieren, "Pencil beam interferometer," US Patent 4,498,773 (1985).
[29] P. Z. Takacs, S. K. Feng, E. L. Church, S. Qian, and W. Liu, "Long Trace Profile Measurements On Cylindrical Aspheres," Proc. SPIE 966, 354 (1989); doi:10.1117/12.948082.
[30] E. Debler and K. Zander, "Measurement of evenness on optical plane surfaces with autocollimator and pentagon prism," PTB-Mitteilungen 90(5), 339-349 (1980).
[31] G. Centers and V. V. Yashchuk, "Literature Review of Pencil Beam Interferometry and the LTP Operating Principle," Light Source Beam Line Note LSBL-1293 (ALS, Berkeley, August 20, 2016); available upon request.
[32] G. Centers and V. V. Yashchuk, "Generalized Derivation of Pencil Beam Interferometry and New 4-Peak LTP Mode," Light Source Beam Line Note LSBL-1296 (ALS, Berkeley, August 22, 2016); available upon request.
[33] J. W. Goodman, *Introduction to Fourier Optics*, 3rd ed., Roberts & Co, Englewood (2005).
[34] S. Qian and P. Takacs, "Precise angle monitor based on the concept of pencil-beam interferometry," Proc. SPIE 4101, 263-272 (2000).
[35] S. C. Irick, "Determining surface profile from sequential interference patterns from a long tracer profiler," Rev. Sci. Instrum. 63, 1432 (1992); doi: 10.1063/1.1143035.
[36] V. V. Yashchuk, Positioning errors of pencil-beam interferometers for long-trace profilers, Proc. SPIE 6317, 6317 0A-1-12 (2006).
[37] Z. Ali, N. A. Artemiev, C. L. Cummings, E. E. Domning, N. Kelez, W. R. McKinney, D. J. Merthe, G. Y. Morrison, B. V. Smith, and V. V. Yashchuk, "Automated suppression of errors in LTP-II slope measurements with x-ray optics," Proc. SPIE 8141, 81410O-1-15 (2011); http://dx.doi.org/10.1117/12.894061.
[38] S. C. Irick, "Long trace profiler survey results," Proc. SPIE 3782, 275 (1999); doi:10.1117/12.369237.